Title	Numerical Simulation of Alveolar Bone Regeneration and Angiogenesis - Building a Coupled Model -
Author(s)	Kitamoto, Akihiro; Nagayama, Katsuya; Matsuo, Masato
Issue Date	2015-12-18
URL	http://hdl.handle.net/10228/5563
Rights	

The 6th TSME International Conference on Mechanical Engineering
16-18 December 2015
Cha-Am, Phetchaburi, Thailand

Harmonized Engineering Technologies

BME007

Numerical Simulation of Alveolar Bone Regeneration and Angiogenesis - Building a Coupled Model -

Akihiro Kitamoto[1], Katsuya Nagayama[1*], and Masato Matsuo[2]

[1] Kyushu Institute of Technology, 680-4 Kawazu, Iizuka, Fukuoka, 820-8502, Japan
[2] Kanagawa Dental University, 82 Inaokacho, Yokosuka, Kanagawa, 238-8580, Japan
[*] Corresponding Author: nagayama@mse.kyutech.ac.jp, Tel & Fax 81-948-29-7778

Abstract

Alveolar bone is the substance that supports teeth. Regeneration of alveolar bone after tooth extraction is known to be adaptively constructed with Ca^{2+}consumption, which is secreted from the blood vessels. Thus, there is a strong relation between alveolar bone regeneration and angiogenesis and Ca^{2+} secreted from blood vessels. In addition, bone formation is affected by the mechanical force around it and shape remodeling by osteoblasts and osteoclasts. Therefore, in this study, an angiogenesis model, a Ca^{2+} transport model, stress analysis model, and reaction-diffusion model are constructed and calculated at the same time as the coupled analysis model of bone formation. Thus, the bone regeneration model is constructed using the above factors and compared with the data or images of the actual phenomena.

Keywords: Numerical Simulation, Bone Formation, Angiogenesis

1. Introduction

Currently in clinical dentistry, reproduction dentistry to regain lost bone because of periodontal disease has been studied extensively. Alveolar bone is the substance that supports teeth in the jawbone and buffers occlusal pressure. Bone is regenerated using Ca^{2+} secreted from the blood vessels, chemically changing into the principal component of bone known as hydroxyapatite. Furthermore, the internal and external structures of the bone are influenced by the mechanical force around it.

Various mathematical models of bone formation have been previously proposed. However, few studies have examined a mathematical model highlighting the relationship between angiogenesis and bone formation. Therefore, in this study, we constructed a coupled bone regeneration analysis model including angiogenesis and various other factors using the particle model. The characteristics of angiogenesis in the bone regeneration process are simulated using the coupling angiogenesis and bone formation model. In addition, the reaction-diffusion model and stress analysis model were incorporated into the coupled bone regeneration model to simulate as close as possible, the internal and external structure of the bone.

2. Analysis Object

Figs. 1 and 2 were obtained from bone regeneration experiments [1]. Mandibular premolars were extracted from beagle dogs. The gingival flap was then sutured. Microvascular resin injection was performed after 14, 30, and 90 days. In this study, a mathematical model was constructed for qualitative and/or quantitative comparison.

Fig. 1 Object of analysis (8 mm × 4 mm)

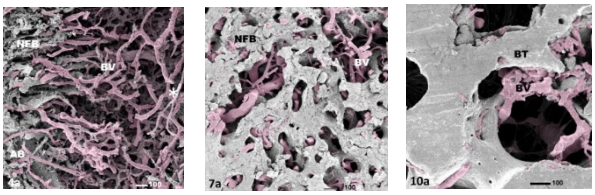

(a) day 14 (b) day 30 (c) day 90

Fig. 2 Images post-surgery (1 mm × 1 mm)

3. Methods

Analyses in this study were performed using the particle model. Positional relationship is not constrained between the particles in this model, thereby allowing complex analysis of the data.

Regeneration of alveolar bone is influenced by many factors such as angiogenesis, Ca^{2+} secreted from blood vessels, and the surrounding mechanical environment. The models for each factor influencing bone formation are described below.

BME007

3.1 Angiogenesis Model

Bone regeneration is considerably affected by angiogenesis because the blood vessels supply the nutrients necessary for bone formation [1-5]. Angiogenesis is the formation of new blood vessels by extending and repetitively migrating and branching vascular endothelial cells. In Fig. 1, the interior of the alveolar bone shows blood clots at the center due to bleeding following tooth extraction; blood vessels extend toward this section. Concurrent with angiogenesis, Ca^{2+} is secreted from the blood vessels. Ca^{2+} in the surrounding area is used for bone regeneration. Because blood vessels extend toward the center of the tooth, as shown in Fig. 1, higher incentive value of angiogenesis is arranged as closer to the center in the entire area in the initial state.

The growth processes of blood vessels in this model are as follows: First, the surrounding blood vessels are examined. Next, the particle with the highest incentive value is selected in the direction of elongation [0–30 (deg)] or branch [60–80 (deg)]. Then, blood vessels extend toward the selected particle with the highest incentive value. In addition, angiogenesis is adjusted to rule out duplicate or converging vessels by monitoring the density of particles. Because the growing speed of blood vessels varies with platelet-rich plasma (PRP) [1-4], it was set as a variable in the analysis.

3.2 Ca^{2+} Transport Model

As described in section 3.1, Ca^{2+} is secreted from newly formed blood vessels and diffused throughout the entire area. The equation we used for the Ca^{2+} transport model is

$$\frac{\partial A}{\partial t} = d_A \nabla^2 A - \frac{1}{\beta}\frac{\partial \rho}{\partial t} \ , \qquad (1)$$

where A is the Ca^{2+} concentration, t is the time, ρ is the bone density, d_A is the diffusion coefficient, and β is the mass ratio of Ca^{2+} and bone. The left-hand side represents the change in Ca^{2+} concentration with respect to time. The first term on the right side represents the diffusion of Ca^{2+}. The second term on the right side represents Ca^{2+} consumption, and it calculates the amount of Ca^{2+} that is consumed during the bone formation.

Ca^{2+} that diffuses into the area changes to hydroxyapatite, which is the main component of bone and is calculated as

$$10Ca(OH)_2 + 6H_3PO_4 \rightarrow Ca_{10}(PO_4)_6(OH)_2 + 18H_2O \qquad (2)$$

Under normal conditions, Ca^{2+} concentration in the blood is between $8.8 - 10.0\ [\mathrm{mg/dl}]$. Therefore, in this analysis, Ca^{2+} concentration in the blood is set as a boundary condition of constant value at $10.0[\mathrm{mg/dl}]$. The boundary condition of the analysis region is set as free because Ca^{2+} flows to the exterior.

3.3 Stress Analysis Model

Bone structure adapts to the load environment because suitable mechanical stimulus encourages bone growth. It has been reported that strain energy effects bone growth with respect to strength or bone density [6-8].

Alveolar bone is maintained because of stimulation by the force of biting. Therefore, in the analysis of alveolar bone regeneration, the distribution of stress on the bone is important. Therefore, in this study, the stress analysis of the newly formed bone is performed using the balance equation of force, which is shown as

$$\frac{\partial \tau_{xy}}{\partial x} + \frac{\partial \sigma_y}{\partial y} + \frac{\partial \tau_{yz}}{\partial z} = 0 \ , \qquad (3)$$

where σ is the normal stress, and τ is the shear stress. Incidentally, this analysis assumed isotropic elastic incompressible medium for simplicity.

The process of stress analysis is as follows: First, forced displacements were subjected to the boundary particle, and the other boundary particles were set as free boundary. Second, the strain ε is derived from each part of the displacement, which is transmitted to the entire area by an external force. Next, strain energy U distribution was calculated using the following equation:

$$U = \frac{1}{2} E \varepsilon^2 \ , \qquad (4)$$

where E is Young's modulus. Young's modulus was derived from the relation:

$$E = c\rho^3 \qquad (5)$$

(Carter and Hayes, 1977) [6-8]. Young's modulus when bone density is $0.5\ [\mathrm{mg/mm^3}]$, is assumed to be 480 [MPa]. Poisson's ratio is assumed to be 0.23.

3.4 Reaction-diffusion System Model

In order to produce the structure of bone in our analysis, the reaction-diffusion model was introduced. It is essential for forming the scaffold of bone that is not influenced by small differences in the initial field. Therefore, the reaction-diffusion model was based on Turing's model [8-10]. Turing's model changes a uniform field into a non-uniform and biological field using an activator and inhibitor. They are diffused while mutually suppressing each other. In bone formation, osteoblasts and osteoclasts correspond to activators and inhibitors, respectively. In our analysis, osteoclasts were assumed to have already diffused throughout the entire area because the diffusion coefficient of the osteoclast is large compared with that of the osteoblasts. In addition, instead of suppressing the effect of the interaction of two factors, forcible suppression is performed by assigning upper $[0.5(\mathrm{mg/mm^3})]$ and lower $[0.0(\mathrm{mg/mm^3})]$ limits for bone density. Therefore, considering that osteoblasts transform into bone, the equation of bone formation is assumed by using bone density ρ as follows:

BME007

$$\frac{d\rho}{dt} = d_\rho \nabla^2 \rho \qquad (0.0 \le \rho \le 0.5) \ , \tag{6}$$

where d_ρ is the diffusion coefficient. The boundary conditions of the diffusion of bone density were set to periodic boundary conditions.

3.5 Bone Formation Model

Huiskes and coworkers designed a model that relates bone formation strain energy U and Young's modulus E:

$$\frac{dE}{dt} = C(U - U_h) \ , \tag{7}$$

where t is time, C is a constant, U_h is the homeostatic strain energy.

In this study, it is assumed that each factor of bone regeneration is independent of each other. Therefore, bone formation is defined as the growth of bone density and is modeled using the following equation:

$$\frac{\partial \rho}{\partial t} = C_A (A - A_h) + C_U (U^{\frac{1}{3}} - U_h^{\frac{1}{3}}) + d_\rho \nabla^2 \rho \qquad (0.0 \le \rho \le 0.5) \ , \tag{8}$$

where A is Ca^{2+} concentration, U is strain energy, d_ρ is the diffusion coefficient, C_A and C_U are constants, A_h is assumed as the homeostatic Ca^{2+} concentration 3.0 [mg/dl] of saliva, and U_h is the homeostatic strain energy, which is a different value for each patient. On the right side of Equation (8), the first term shows that the larger the bone density, the more the bone growth. If the Ca^{2+} concentration is smaller than the homeostatic value A_h, bone dissolves. The second term on the right-hand side of Equation (8) indicates that strain energy becomes a burden on local bone and promotes bone growth. The third term on the right-hand side of Equation (8) indicates the effect of reaction and diffusion on bone formation.

4. Results and Discussion

The computational domain was set to a cube of $1[\mathrm{mm}^3]$ to eliminate the influence of boundaries. In our model, 90 particles were arranged in various directions; therefore, a total of 729,000 particles covered the entire area. Time step width was set to $500[\mathrm{steps/day}]$. The total number of days for analysis was 90[days].

4.1 Analysis of Bone Shape Optimization

To observe the nature of the mechanical factors and reaction-diffusion system in the optimization of the bone structure, Ca^{2+} concentration was assumed to be always maintained at equilibrium, i.e., $A = A_h$, at any time and region. Therefore, it is calculated ignoring the first term on the right-hand side of Equation (8).

In the initial state, bone density is arranged at random in the range of $0 \le \rho \le 0.001[\mathrm{mg/mm}^3]$ in the entire area as shown in Fig. 3. This arrangement is regarded as a uniform field because each bone density value in the initial state is small throughout.

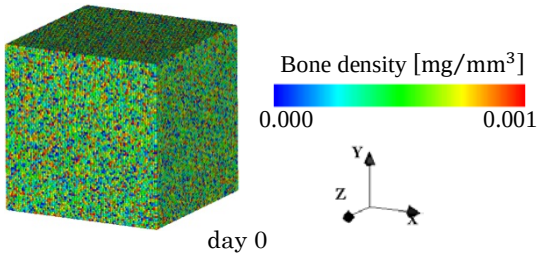

Fig. 3 Initial state of bone density

Here, enforced displacements of the same magnitude are shown perpendicular to the respective boundary planes of the cube in the direction of compression. Fig. 4 shows the analysis results of bone formation over time under these conditions.

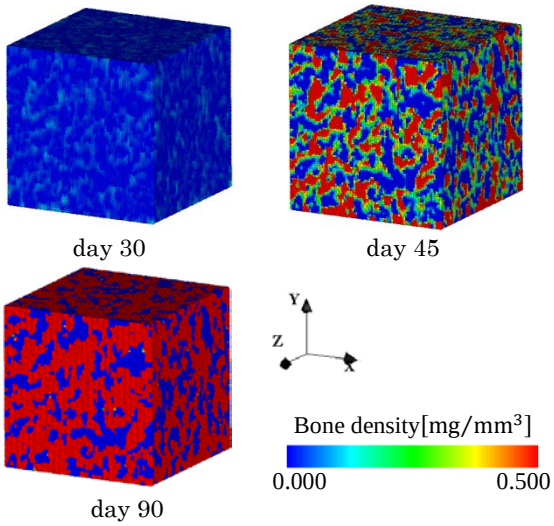

Fig. 4 Bone formation analysis in same-enforced displacement in all directions

It is observed from Fig. 4 that the amount of change in bone density during relatively early days is smaller than that during later days. Low bone density in the early days also corresponds with low strain energy. Therefore, the value of the reaction-diffusion term is larger than the value of the strain energy term in the bone formation Equation (8). Moreover, the scaffold formation of bone is created by the reaction-diffusion and strain energy during the early stages. Subsequently, strain energy becomes dominant when the bone density increases; thus, bone density grows considerably in locations where the value of strain energy is relatively large. By day 90, bone density had reached equilibrium.

Fig. 5 shows the analysis results of bone formation whose load environment is different from that of Fig. 4. The respective large enforced displacements are given in the direction of X in Fig. 5 (a) and of Y in Fig. 5(b).

BME007

Both of them show results at day 90, and the bone growth had reached an equilibrium state.

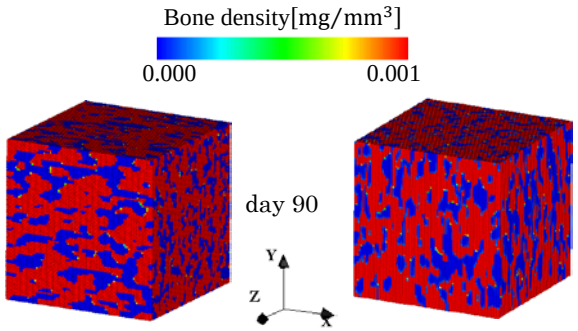

(a) Respective large X-enforced displacement

(b) Respective large Y-enforced displacement

Fig. 5 Bone formation analysis with different enforced displacements in each direction

In the results of Fig. 4, the bone formed almost isotropically in three directions. However, in Fig. 6, it can be confirmed that bone formation oriented in the direction of the largest enforced displacement amount, X in (a) and Y in (b). In addition, the bone area is large in planes that are perpendicular to the direction of large amounts of enforced displacement compared with other sections.

Based on the above two results on morphological characteristics, it is concluded that bone is formed to assist the surrounding mechanical environment.

4.2 Angiogenesis and Ca^{2+} Transport Analysis

The angiogenesis model and Ca^{2+} transport model, which influence bone regeneration, are analyzed in this section. Bone formation is not analyzed here because of the viewing characteristics of angiogenesis and Ca^{2+} transport. Therefore, the second term on the right-hand side in Equation (1), which represents the consumption of Ca^{2+} during bone formation, is ignored.

The calculation condition was as follows: In the initial state, nine of the origin particles of angiogenesis are arranged in an XY plane. Blood vessels extend in the range of $0.01 - 0.13[\mathrm{mm}]$ once a day as time progresses. Then, they branch once, while blood vessels extend 20 times. When a blood vessel reaches the opposite plane, extension is stopped. When it exceeds any of the four side planes by angiogenesis, the blood vessel is deflected on the surface. Ca^{2+} diffusion was calculated for each step. The coefficient of Ca^{2+} is set to $1.0 \times 10^{-13}[\mathrm{m^2/s}]$, which is smaller than usual [11], to see the diffusion phenomenon more easily because Ca^{2+} consumption is not considered here. The boundary conditions of Ca^{2+} are set as free because the analyzed area is a tooth extraction socket as shown in Fig. 1. Therefore, Ca^{2+}, which reaches the boundary limits of this analysis, flows out of the area.

Fig. 6 shows the analysis results of angiogenesis and Ca^{2+} transport under the above calculation conditions.

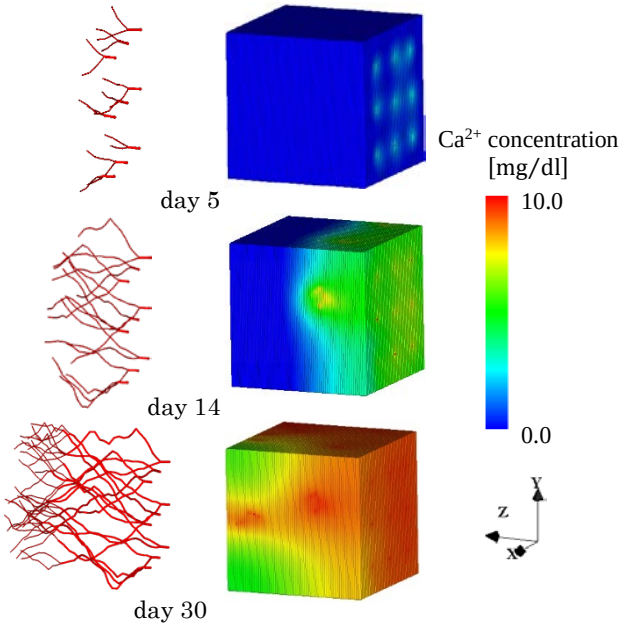

Fig. 6 The analysis of angiogenesis and Ca^{2+} transport

In the analysis results of Fig. 6, blood vessels have grown from the starting points to cover the entire area while continuing to extend and branch. They have also maintained a suitable distance from each other without contact. In addition, Ca^{2+} is diffused to the periphery around the blood vessels and spread throughout the entire area. The blood vessels stopped growing when they reached the opposite side of the point of origin. All blood vessels, including the new blood vessels formed from branching, reached the opposite side and then angiogenesis stopped completely. This is when an equilibrium state of angiogenesis was achieved. Ca^{2+} diffusion lasted for a while after reaching an equilibrium state of angiogenesis. Ca^{2+} was equilibrized when the Ca^{2+} concentration was 10.0 [mg/dl] over the entire region, which is the Ca^{2+} concentration in blood.

4.3 Coupled Analysis Including Angiogenesis and Mechanical Factors

In this section, overall coupled analysis considering angiogenesis and mechanical factors for 30 days is performed using Equation (7). Here Ca^{2+} concentration is assumed to be always maintained at equilibrium; i.e., $A = A_h$ at any time and region because the increase in bone density is still small after 30 days. However, Volkmann's canals, which are created under the influence of angiogenesis, are considered. At day 30, bone density is still small; therefore, bone is not formed near the blood vessels due to intense flows by Ca^{2+} secretion, as shown in Fig. 1(b). Therefore, we conclude that bone is not formed in particles next to the blood vessels.

Under initial conditions, nine origin particles of blood vessels are arranged in an XY plane as discussed in section 4.2. Bone density is arranged over the entire area as small uniform field of random, i.e., $0 \leq \rho \leq$

0.001 [mg/mm^3], as described in section 4.1. In addition, the enforced displacements of the same magnitude are shown perpendicular to the respective boundary planes of the cube in the direction of compression.

Fig. 7 is the analysis results of coupled analysis under the above calculation conditions. Fig. 7(a) shows both blood vessels and bone in any of the five sections. Fig. 7(b) shows both blood vessels and bone in the center section. Both of them display results 30 days after surgery.

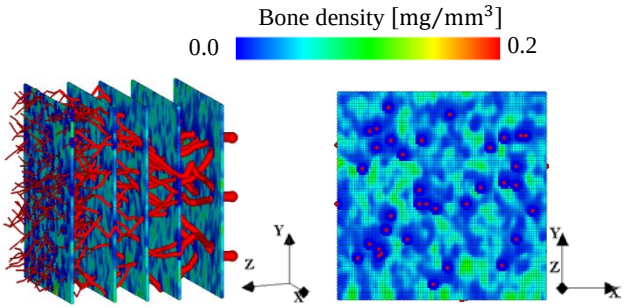

(a) Any of the five sections (b) Center sections

Fig. 7 Coupled analysis of angiogenesis and mechanical factors

In the analysis results of Fig. 7, it can be confirmed that blood vessels have grown from the starting points to cover the entire area while continuing to extend and branch, and bone that was formed had a small density. Moreover, Figs. 4 and 5 show that Volkmann's canals were created by mechanical factors However, it can be concluded that some of them were created by the influence of blood vessels. In summary, bone formation requires the influence of both angiogenesis and mechanical factors.

In this analysis, angiogenesis affects only the shape of the bone formed, leading to the creation of Volkmann's canals, but the Ca^{2+}, which is secreted from blood vessels, was not examined. However, the amount of Ca^{2+} supply should have an effect on bone formation to a certain degree. In future studies, we will perform coupled analysis that takes into account the influence of Ca^{2+} concentration in this model.

5. Conclusions

Major factors of bone regeneration were modeled and analyzed in this study. In the angiogenesis model, blood vessels grew from the starting points and covered the entire area of the vessels. In the Ca^{2+} transport model, Ca^{2+} is diffused into the periphery around the blood vessels and spread throughout the entire area. In the bone formation analysis model, which is affected by mechanical factors but not by angiogenesis, the morphological effect (optimization of bone shape by the surrounding load environment), of the mechanical factor and reaction-diffusion factor in bone formation are demonstrated. In bone formation analysis, in which both angiogenesis and mechanical factors are considered but not Ca^{2+} transport, Volkmann's canals were created around blood vessels.

In the future, coupled analysis examining Ca^{2+} transport over a wider area will be performed. This will allow us to study the effects of angiogenesis in bone formation under different growing speeds of the blood vessels using PRP. In addition, patient-specific parameters such as homeostatic strain energy will be considered.

6. Acknowledgement

This work was supported by JSPS KAKENHI Grant Number 26420202.

7. References

[1]Masato MATSUO, Toshimitsu OKUDERA, Mariko IWAMIYA, Regeneration of Microcirculation and Alveolar Bone after Application of Platelet-Rich Plasma, Microvaslular Reviews and Communications IV, 2011, p.12-17.

[2]Toshimitsu OKUDERA, Masato MATSUO, Mariko IWAMIYA, Alveolar Bone and Microvascular Changes after Synthetic Bone Regeneration Therapy Using Platelet-Rich Plasma, Journal of Japanese Society of Oral Implantology, 2010, vol.23, no.3, p.18-25.

[3] Matsuo M., Iwamiya M., Saito M., Todoki K. and Kishi Y.: Regeneration processes of microcirculation of alveolar bone after synthetic bone graft using platelet-rich plasma(PRP). *Bull. Kanagawa Dent. Col*, 35: 25-33, 2007.

[4]Okudera T., Matsuo M. and Iwamiya M.: Alveolar bone and microvascular changes after synthetic bone regeneration therapy using platelet-rich plasma (PRP). *J. Jpn. Soc. Oral. Implan*t., 23: 18-25, 2010.

[5]Matsuo M., Nakamura T., Su C., Shimomura T., Kisara K., Matsuda D., Kishi Y. and Takahashi K.: Microvascular architecture of alveolar bone after guided bone regeneration with a a resorbable membrane. Jpn. J. Oral. Biol., 40: 656-661, 1998.

[6]Ronald Ruimerman, Modeling and remodeling in bone tissue: Technische Universiteit Eindhoven, 2005. Proefschrift. - ISBN 90-386-2856-0.

[7]Carter, D. R. and Hayes, W. C., The Compressive behavior of Bone as a Two-Phase Porous Structure, J. Bone Joint Surgery, 59, (1977), pp.954-962.

[8]Yoshiki Honma, Taiji ADACHI, Kenichi TEZUKA, Yoshihiro TOMITA, Computational simulation for trabecular regeneration in cancellous bone defect using a reaction-diffusion system model, The Japan Society of Mechanical Engineers,04-40(2004),327-328.

[9]Yoh Iwasa (2008) *Theoretical Biology*, Tokyo: Kyoritsu Shuppan.

[10]Miura, M., H. Sakaguchi & M. Matsushima (2000) Reaction-diffusion modelling of bacterial colony patterns. *Physica A* 282: 283-303.

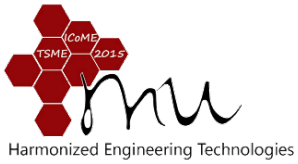

BME007

[11] Hitomi T., Takeda N. and Iriya K.: Calculation of Calcium Diffusion Coefficient of Cement Hardenings Using Minute Pore Data, *Obayashigumi gizyutsukennkyuusyohou(A house magazine of Obayasi Co., Ltd)*, 73, 2009.